# Adding a Length Scale to the Polyamorphic Ice Debate

C. A. Tulk,[1] R. Hart,[2] D. D. Klug,[3] C. J. Benmore,[2] and J. Neuefeind[1]
[1]*Oak Ridge National Laboratory, Oak Ridge, Tennessee 37831, USA*
[2]*Argonne National Laboratory, Argonne, Illinois 60438, USA*
[3]*Steacie Institute for Molecular Sciences, National Research Council of Canada, Ottawa ON, K1 A 0R6, Canada*
(Received 23 January 2006; published 14 September 2006)

X-ray scattering and molecular dynamics simulations have been used to correlate the short range oxygen-oxygen structure with the intermediate range ordering (IRO) upon annealing very high density amorphous ice. While it is clear that the IRO that defines the network structure breaks down continuously to a minimum level, where there are weakened correlations extending beyond 7 Å, at this point the local structure (O-O-O angles) is observed to change abruptly, allowing a continuous reemergence of a new IRO network. This is very different from a classic first order transition and helps reconcile previous data.

DOI: 10.1103/PhysRevLett.97.115503 PACS numbers: 62.50.+p, 61.12.Ld, 61.25.Em, 61.43.−j

In network bonded systems, such as the highly directional hydrogen bonding in ice, it is known that a small set of narrowly defined oxygen-oxygen-oxygen (O-O-O) angles allows for the formation of a crystalline lattice, and the long range repetition of the local structural units are then defined by a set of crystallographic symmetry operations. Intermediate values between the ''ideal'' bond angles will energetically hinder the long range repetition of the local structural units and, thus, restrict the length scale of the ordering. This leads to a high degree of disorder that results in the well known forms of amorphous ice. These ices have historically been referred to as low density amorphous (LDA), high density amorphous (HDA), and, more recently, very high density amorphous (VHDA) forms [1,2]. Amorphous ice takes on structures that are characterized on a local level by distributions of bond angles. Amorphous ice also shows ordering that extends over several hydrogen bond lengths into the intermediate range, as has been demonstrated in recent experiments by Guthrie *et al.* [3] and Koza *et al.* [4]. In those studies, the structural properties of the VHDA, HDA, and LDA ice forms, the relative extent of the correlations in each, and, specifically, the likeness of a particular state of annealed VHDA and unannealed HDA have been discussed. However, the determination of local bond angles is fundamental to fully characterizing amorphous structures, and, considering the relative neutron weighting [5] of the partial structure factors, this O-O-O angle information is very difficult to obtain using the neutron data alone. Below, we present a detailed view of the structural transformation process upon annealing on both a local scale (the near neighbor O-O-O angles) and on the intermediate length scale and emphasize the important relation between the two.

X-ray structure factors $S_x(Q)$ of amorphous ice are heavily weighted toward the oxygen-oxygen correlations [3] and exhibit a first diffraction peak (FDP) located between 1.7 and 2.36 $\text{Å}^{-1}$ [6,7]. As such, the position, width, and amplitude of this FDP are often associated with the packing of the structural units and the spatial range, or extent, of the ordering in the material [8,9]. It has become evident that the peak position and shape of the FDP in the structure factor of amorphous ice forms varies significantly [4,5,10], and peak shift parameters have been used to account for this feature of the diffraction data [11]. Since submission of this Letter, other authors have reported experimental observation of the FDP position [12]. We interpret this shift in the FDP as a variation in the packing of the network and not a simple expansion or contraction at constant structure [13]. As such, a wide variation in structures is possible from low density amorphous ice through a continuum of higher density states to the very high density amorphous structure, as the sample's pressure/temperature environment changes [3–5,14–20]. Conversely, however, Raman spectroscopic studies seem to indicate abrupt changes in the structure [21]. Recent fits of a simple two state model to neutron diffraction data have been taken as evidence for its validity [11,12]; however, the quality of the fits based on statistical noise levels and data analysis has been questioned [13]. These structural changes are known to be reversible upon recompression of the low density form at low temperature [21,22].

In this study, VHDA ice samples have been produced at the National Research Council of Canada by pressurizing $D_2O$ ice Ih at liquid nitrogen temperature to 18 kbar, followed by reducing the pressure to 12 kbar and *in situ* annealing the sample at 160 K for 15 minutes, and cooling back to liquid nitrogen temperature and then decompressed to ambient pressure. The density of the sample was observed to be 10% greater than that of high density amorphous ice produced previously. The recovered sample was stored in liquid nitrogen and shipped to the Advanced Photon Source at Argonne National Laboratory. The initial diffraction data set confirms production of a very dense amorphous structure.

Diffraction data, i.e., x-ray $S(Q)$'s, were collected using high energy x rays (115 keV) from sector 11-ID-C at the Advanced Photon Source (APS). Samples were cold loaded (77 K) into an aluminum sample holder with a thin Kapton window and placed in a He cryostat. The procedure for correcting the data has been outlined previously [23]. Initial data were collected immediately after loading the sample at 40 K to characterize the unannealed ‘‘as produced‘‘ structure.

Four data sets were collected from 0.4 to 10 Å$^{-1}$ at each temperature of 100, 105, and 110 K, and ten such data sets were collected at 115 K. Between each anneal, the sample was cooled to 40 K, and another much longer data set was collected to a maximum $Q$ value of 20 Å$^{-1}$. The resulting low temperature structure factors are shown in Fig. 1. The total x-ray structure factor for water is heavily weighted toward the oxygen-oxygen form factor and much less so to the oxygen-hydrogen and the hydrogen-hydrogen form factors [13,24]. We note here that the neutron oxygen-oxygen partial contributes only 9% of the total neutron structure factor, making the interpretation of the subtle effects reported here much more difficult using neutron data. The structure factors of the low density amorphous forms have been characterized by a FDP at roughly 1.7 Å$^{-1}$, while the very high density forms show a sharp peak in the region of 2.36 Å$^{-1}$. The FDP position shifts between these values as the density varies, and the transformation progresses, as has been reported previously [5,10]. We cannot reliably interpret the increased low $Q$ signal that is initially present in the highest density unannealed forms due to the limited low $Q$ range measured. We therefore reserve further comment on these conclusions of Koza *et al.* [4].

Molecular dynamics simulations were performed using the extended simple point charge water potential employing a simulation cell of 1536 water molecules in an ice Ih lattice, with the water molecules placed to yield a minimum dipole moment for the simulation cell, and an orientationally disordered ice lattice. Simulations were carried out using the DLPOLY code [25] and employed the Nose-Hoover (Melchionna) anisotropic $N$-$P$-$T$ ensemble. The sample was annealed at 80 K and then the pressure was increased to 20 kbar, maintaining the sample temperature at 80 K. The sample was then heated in 10 K steps to 200 K. Typical runs were carried out for ~0.15 ns using a time step of 1 fs. The pressure was then decreased to 1 bar in 4 steps, and annealing calculations were carried out with the sample at 1 bar with sample temperatures in the range 80–220 K. These annealing simulations were carried out using two runs of 50 000 time steps at each temperature with the sample equilibrated and temperature scaled for the first 10 000 time steps and data collected for analysis in the last 50 000 time steps. The volume changes after the first 10 000 time steps were essentially negligible (<0.2%).

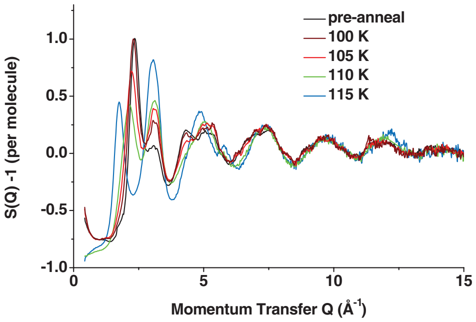

FIG. 1 (color). Structure factor functions measured at various points during the transformation process. The data set labeled ‘‘preanneal’’ is structure factor measured at 40 K of the ‘‘as produced‘‘ VHDA amorphous ice structure after loading into the cryostat. The other structure factors have been measured after each annealing process and quenching to 40 K. The data set labeled 115 K represents the structure factor from the LDA ice form. The range from 15 to 20 Å has been used for normalization.

Fourier transforms of the experimentally determined x-ray diffraction structure factors $S(Q)$’s, a subset of which is shown in Fig. 1, yield the x-ray radial distribution functions $G_x(r)$. This inversion was performed using a Lorch modification function to minimize Fourier artifacts [26]. The weighted pair distribution function $G_x(r)$ and the differential distribution function $D_x(r)$ function are plotted in Figs. 2(a) and 2(b); here $D_x(r) = 4\pi r(\rho(r) - \rho_o)$, where $G_x(r) = \rho(r)/\rho_o$ (as defined by Dejus *et al.* [27] and where the $\rho(r)$ is the x-ray weighted average number density at distance $r$ and $\rho_o$ is the bulk average number density). This figure illustrates the local ordering defined by the nearest neighbor O-O correlation length located at 2.83 Å for run number 1 (VHDA) and 2.76 Å for run number 23 (LDA). Other correlations making up the local ordering, out to 7 Å, are also shown. More importantly, however, the evolution of the local structure can be qualitatively followed as the density changes, as in Fig. 2(a). The line overlaid on the data outlines the distribution centers of the next-nearest neighbor oxygen correlations. Several data points along this line are also shown as the open circles in Fig. 2(b). In the lower density forms, the distribution centers are located at a distance of 4.2 Å. The position of this line for these lower density forms, above run number 15, was determined from the zero value in the first derivative of the radial distribution function. At run number 15 and lower, the first derivative of the radial distribution function no longer

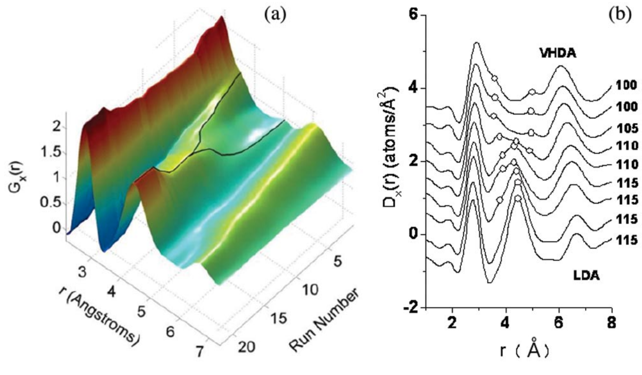

FIG. 2 (color). (a) The short range ordering region of the $G_x(r)$ functions. Increasing run number represents decreasing sample density. (b) $D_x(r)$ showing the locations of some of the data points (open circles) along the line overlaid on the plots in (a).

crosses zero, since the O-O distributions have broadened significantly and have merged to form a well defined shoulder on the first peak. At this point, the lines represent the distribution centers by following the inflection points in the derivative of each radial distribution function. In the first radial distribution function, the lower distance branch represents the average distance of oxygen atoms that have been forced close to the first coordination shell in the VHDA sample preparation [3,28]. The higher distance branch is located just above 5 Å. It is clear that a shift in the first diffraction peak does not indicate an expansion without structural change.

During the experiment, the density decreases and the branches are observed to converge, as discussed later and seen more clearly in Fig. 4. Full convergence of the two O-O distributions to form a single second correlation shell occurs at run number 10, as the sample density passes through 0.109 atoms/Å$^3$ (as estimated from the location of the principal diffraction peak and the known density of VHDA and LDA ice). For lower density, that is, for run numbers greater than 10, the second coordination shell continues to sharpen.

The average O-O-O angle is determined from the nearest and next-nearest neighbor distances for each of the distribution centers (outlined by heavy lines in Fig. 2) in the next-nearest neighbor distance correlations. O-O-O angles were calculated using distances from measured peaks in the radial distribution function [see the open circles in Fig. 2(b)] and the law of cosines for triangles. The analysis of the molecular dynamics (MD) data was done in the same manner. Two atoms are defined as linked by a hydrogen bond if their distance spanned the range from 2.75 to 2.93 Å (the range covered by crystalline forms of ice with similar densities). For the two end amorphous forms, these angles have been determined experimentally to be 107.2° for the lowest density form (which is close to that of crystalline ice I) and 118.7° and 75.1° for the highest density form (which is close to that of ice VI but, in addition, also covers the hydrogen bonded angular range of ice XII). The values similarly determined for the intermediate density structures are plotted in Fig. 4(a), where the two step convergence of the O-O-O angle branches is illustrated. This stepwise convergence process is indicative of abrupt changes at the local structure, which occur when the sample density is between 0.1150 and 0.107 atoms/Å$^3$.

The evolution of the intermediate range ordering can be seen from the plot in Fig. 3(a) of the experimentally determined total differential distribution function $D_x(r)$. We also plot in Fig. 3(b) the simulated partial radial distribution functions of the oxygen-oxygen correlations as $r^2 g_{OO}(r)$, where $g_{OO}(r)$ is the partial O-O pair distribution function from the MD simulation box. The ordering in the "very" highest density structure and the lowest density structure extends to greater distance than that of the intermediate (HDA) structure [3,4]. Five coordination shells are evident in the very highest density structure, i.e., run number 1, extending to 13 Å. As the density is decreased, the correlations extending beyond 7 Å are observed to decrease in intensity. The degree of intermediate range ordering in the third shell of the very highest density form is observed to break down. This same trend is also quantitatively obtained in the MD simulations [Fig. 3(b)]. This breakdown in the degree of intermediate range ordering occurs smoothly over several data collection runs. At run number 15, the intermediate range correlations are observed to continuously reemerge, to form the fourth and higher coordination shells in the lower density network structure.

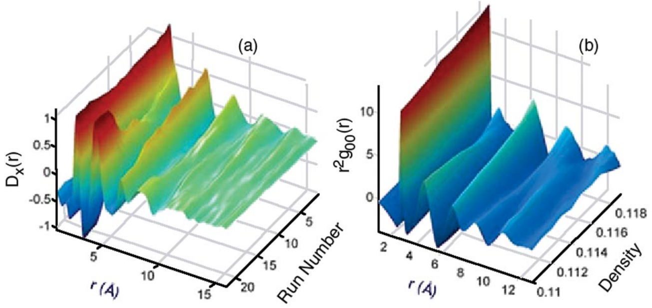

FIG. 3 (color). IRO evolution as the sample structure changes. The experimental data are plotted in (a) and the O-O correlations determined directly from the simulation box are plotted in (b). The increasing run number for the experimental data again represents decreasing density from VHDA at run number 1 to LDA at run number 23.

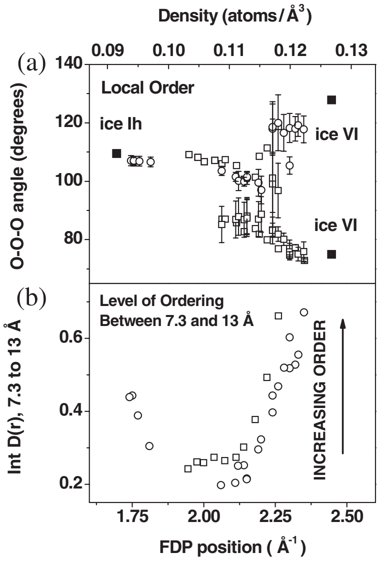

FIG. 4. (a) The experimentally determined and simulated O-O-O angle as a function of the FDP in the structure factor and sample density (as determined by the position of the FDP and the density of the initial very high density form and the final LDA form). (b) The degree of ordering from the measured and simulated differential distribution functions $D_x(r)$, also as a function of the FDP position and sample density. The open squares, solid squares, and open circles represent the simulation data, crystalline data, and experimental data, respectively.

The changes in the intermediate range ordering (IRO) along with changes in the local structure can be simultaneously tracked by plotting the O-O-O angle as a function of the FDP position and the sample density as in Fig. 4(a), along with the integrated absolute value of the differential distribution function $D(r)$ over the range 7.3–13 Å [see Fig. 4(b)]. A smaller integrated value represents a lesser degree of intermediate range ordering.

As the density decreases towards 0.117 atoms/Å$^3$, the intermediate range ordering is observed to decrease continuously as the lower O-O-O angle branch gradually increases and the angle distributions begin to slowly converge. Between densities of 0.117 and 0.107 atoms/Å$^3$, the O-O-O angles converge in a two step manner, first with the higher angle branch abruptly decreasing from 119° to 100°, followed by a second abrupt change as the lower angle branch moves from 85° to 100°; this change in the local ordering occurs at the minimum in the level of IRO. This structural region has a FDP near $Q = 2.1$ Å$^{-1}$. After the O-O-O angle branches converge, the intermediate range ordering reemerges as the low density network forms, and, on a local level, the maximum in the angle distribution slowly moves from 100° to 107° in the lowest density structure.

The structural transformation from the very highest density form to the lowest density form of amorphous ice is primarily characterized by a continuous breakdown in the intermediate range ordering. After significant breakdown of the IRO has occurred, each branch of the O-O-O angle distribution is observed to converge to a single angular distribution. After these changes in the local structure, the degree of intermediate range ordering is again seen to continuously increase as the low density network emerges.

The data presented clearly show that the sample moves through a series of metastable states from the initial VHDA structure through an HDA structure to the final LDA structure during the course of the experiment, and the analysis clearly outlines the structural path of the transition between these amorphous forms. These data further raise serious questions regarding the extent to which these structural changes in amorphous ice forms can be carried over to liquid water, temperature quenched glassy water, and the proposed second critical point.

Finally, Raman spectroscopy of the internal OH vibrations in ice probes intermolecular and intramolecular forces that are principally influenced by the strength and geometry of the hydrogen bonds and is, therefore, considered an indirect largely *local* structural probe. Abrupt changes in the local bonding angles, as shown here, will significantly alter the Raman frequencies, whereas diffraction data, and particularly quantification of the spectral features of the FDP, involve the structural evolution beyond the local level and reflect the changes at greater distances. This behavior of abrupt local changes concurrent with continuous changes on an intermediate length scale distinguishes an amorphous-amorphous ice transformation from crystalline ice transformations, where both short and longer range correlations change discontinuously.

The Spallation Neutron Source is managed by UT-Battelle, LLC, under Contract No. DE-AC05-00OR22725 for the U.S. Department of Energy. The work performed at the APS and IPNS Divisions of Argonne National Laboratory was supported by the U.S. Department of Energy, under Contract No. W-31-109-ENG-38.

[1] O. Mishima, L. D. Calvert, and E. Whalley, Nature (London) **310**, 393 (1984).
[2] T. Loerting, C. Salzmann, I. Kohl, E. Mayer, and A. Hallbrucker, Phys. Chem. Chem. Phys. **3**, 5355 (2001).
[3] M. Guthrie, C. A. Tulk, C. J. Benmore, and D. D. Klug, Chem. Phys. Lett. **397**, 335 (2004).
[4] M. M. Koza *et al.*, Phys. Rev. Lett. **94**, 125506 (2005).
[5] M. Guthrie *et al.*, Phys. Rev. B **68**, 184110 (2003).
[6] L. Bosio, G. P. Johari, and J. Teixeira, Phys. Rev. Lett. **56**, 460 (1986).
[7] M. A. Floriano, E. Whalley, E. Svensson, and V. F. Sears, Phys. Rev. Lett. **57**, 3062 (1986).
[8] S. R. Elliot, Nature (London) **354**, 445 (1991).
[9] P. S. Salmon, R. A. Martin, P. E. Mason, and G. J. Cuello, Nature (London) **435**, 75 (2005).
[10] C. A. Tulk *et al.*, Science **297**, 1320 (2002).
[11] S. Klotz *et al.*, Phys. Rev. Lett. **94**, 025506 (2005).
[12] R. J. Nelmes *et al.*, Nature Phys. **2**, 414 (2006).
[13] C. A. Tulk, C. J. Benmore, D. D. Klug, and J. Neuefeind, Phys. Rev. Lett. **96**, 149601 (2006).
[14] G. P. Johari and O. J. Anderson, J. Chem. Phys. **120**, 6207 (2004).
[15] A. K. Soper, Science **297**, 1288 (2002).
[16] B. Guillot and Y. Guissani, J. Chem. Phys. **119**, 11 740 (2003).
[17] R. Martonak, D. Donadio, and M. Parrinello, Phys. Rev. Lett. **92**, 225702 (2004).
[18] N. Giovambattista, H. E. Stanley, and F. Sciortino, Phys. Rev. Lett. **94**, 107803 (2005).
[19] R. Martanok, D. Donadio, and M. Parrinello, J. Chem. Phys. **122**, 134501 (2005).
[20] M. M. Koza, H. Schober, H. E. Fischer, T. Hensen, and F. Fujara, J. Phys. Condens. Matter **15**, 321 (2003).
[21] O. Mishima and Y. Suzuki, Nature (London) **419**, 599 (2002).
[22] O. Mishima, J. Chem. Phys. **100**, 5910 (1994).
[23] B. Tomberli, C. J. Benmore, P. A. Egelstaff, J. Neuefeind, and V. J. Honlimaki, J. Phys. Condens. Matter **12**, 2597 (2000).
[24] A. Bizid, L. Bosio, A. Defrain, and M. Oumezzine, J. Chem. Phys. **87**, 2225 (1987).
[25] W. Smith, M. Leslie, and T. R. Forester, *The DL-Poly Users Manual, Version 2.11* (CCLRC Daresbury Laboratory, Daresbury, England, 2003).
[26] E. A. Lorch, J. Phys. C **2**, 229 (1969).
[27] R. J. Dejus, S. Susman, K. J. Volin, D. G. Montague, and D. L. Price, J. Non-Cryst. Solids **143**, 162 (1992).
[28] J. L. Finney, Phys. Rev. Lett. **89**, 205503 (2002).